

Matter-wave collimation to picokelvin energies with scattering length and potential shape control

A. Herbst,¹ T. Estrampes,^{1,2} H. Albers,¹ R. Corgier,³ K. Stolzenberg,¹
S. Bode,¹ E. Charron,² E. M. Rasel,¹ N. Gaaloul,¹ and D. Schlippe^{1,*}

¹*Leibniz Universität Hannover, Institut für Quantenoptik,*

Welfengarten 1, 30167 Hannover, Germany

²*Université Paris-Saclay, CNRS, Institut des Sciences Moléculaires d'Orsay, 91405 Orsay, France*

³*LNE-SYRTE, Observatoire de Paris, Université PSL, CNRS,*

Sorbonne Université 61 avenue de l'Observatoire, 75014 Paris, France

(Dated: January 30, 2024)

We study the impact of atomic interactions on an in-situ collimation method for matter-waves. Building upon an earlier study with ^{87}Rb , we apply a lensing protocol to ^{39}K where the atomic scattering length can be tailored by means of magnetic Feshbach resonances. Minimizing interactions, we show an enhancement of the collimation compared to the strong interaction regime observing a one-dimensional expansion corresponding to $(340 \pm 12) \text{ pK}$ in our experiment. Our results are supported by an accurate simulation, describing the ensemble dynamics, which allows us to extrapolate a 2D ballistic expansion energy of $(438 \pm 77) \text{ pK}$ from our measurements. We further use the simulation to study the behavior of various trap configurations for different interaction strengths. Based on our findings we propose an advanced scenario which allows for 3D expansion energies below 16 pK by implementing an additional pulsed delta-kick collimation directly after release from the trapping potential. Our results pave the way to realize ensembles with hundreds of thousands of particles and 3D expansion energies in the two-digit pK range in typical dipole trap setups required to perform ultra-precise measurements without the need of complex micro-gravity or long-baseline environments.

I. INTRODUCTION

Cooling quantum gases to sub-nanokelvin temperatures has enabled breakthroughs in the fields of quantum sensing [1], quantum information [2] and quantum simulation [3]. Especially in precision sensing and metrology, atom interferometers [4–7] have become a state-of-the-art solution and are used for probing general relativity [8–11], quantum mechanics [12–15], determining fundamental constants [16–18] and measuring inertial effects [19–23]. Interferometers utilizing molasses-cooled atoms, characterized by expansion energies in the range of several microkelvin, offer short experimental cycle times and a high sensor bandwidth [24–26]. Despite these advantages, their velocity spread limits the accessible free fall distance and their systematic uncertainty is typically restrained at a few $10^{-8} (\text{m/s}^2)$ due to wave-front distortions, when the ensemble is expanding within the interferometer beam [27, 28]. In contrast, Bose-Einstein condensates (BECs) [29, 30] offer significant advantages with respect to controlling systematic errors and their dynamic behavior [31, 32]. In optical dipole traps (ODTs), BECs of various atomic species readily achieve expansion energies in the range of a few tens of nanokelvin [33–35], enhancing coherence time and signal-to-noise ratio. However, to meet the demands of future precision experiments, further collimation into the picokelvin regime is required to achieve the long pulse separation times

necessary and to avoid loss of contrast [36–40]. Expansion energies of a few hundred picokelvin have been achieved by direct evaporative cooling [41] and spin gradient cooling [42]. Additionally, advancements using different types of matter-wave lenses have further reduced expansion energies by an order of magnitude [43–45]. In this regime, extended free fall times prior to applying the lens are crucial to minimize atomic interactions, which would otherwise drive the expansion post-lensing [46, 47]. Hence, recent records of a few tens of picokelvin have been realized in unique experimental settings utilizing microgravity [48, 49] or long-baseline devices [47] which both allow for an initial prolonged expansion of the ensemble. In this paper we demonstrate a novel approach to resolve this issue by use of a Feshbach resonance [50, 51] to tailor interactions during the lens and upon release from the trapping potential. Using a ^{39}K BEC in the weak interaction regime, we observe expansion energies below 400 pK in one dimension. Through dedicated theory simulations, we extrapolate this result to two dimensions, yielding a 2D energy below 500 pK. We hence demonstrate a substantial improvement over previous results achieved with the same method and setup using ^{87}Rb [52]. Furthermore, our systematic analysis reveals that the careful adjustment of trapping frequencies and interactions will allow to reach 3D expansion energies below 16 pK, when implementing an additional delta-kick collimation (DKC) pulse [43] after a few milliseconds of free fall. Hence, our method allows for state-of-the-art collimation in typical or even compact quantum optics experiments, without excessive hardware or environmental requirements.

* Email: schlippe@iqo.uni-hannover.de

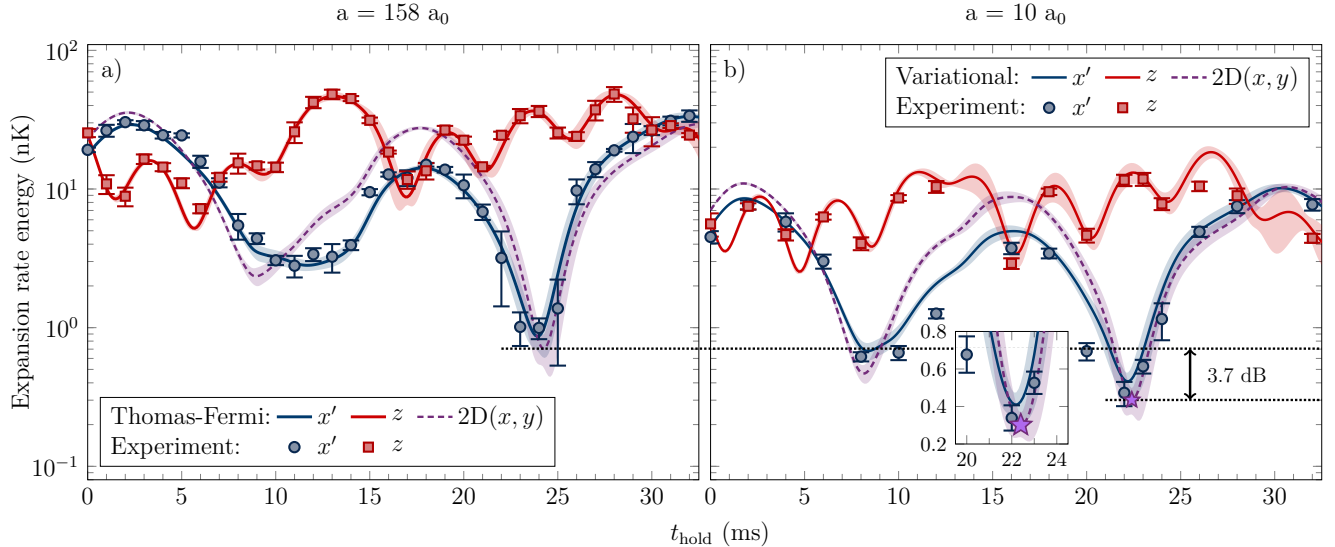


FIG. 1. **Measured and simulated expansion rate energies E^{1D} and simulated 2D expansion energies E^{2D} in the horizontal plane for $158 a_0$ (a) and $10 a_0$ (b) scattering length after 25 ms TOF.** All measurements (points) are obtained within the camera frame, while the error bars arise from the fit uncertainty of the expansion in the individual TOF series (c.f. section IV C). For the $10 a_0$ case we choose a lower sampling rate, allowing to increase the number of points per TOF measurement to resolve the lower expansion energies, effectively. The dynamics of the ensemble are simulated (lines) simultaneously for all directions within the trap frame and are subsequently transformed into the camera frame. For $158 a_0$ we use the Thomas-Fermi approximation, while at $10 a_0$ a variational approach is used (c.f. section IV D). In both cases the shown simulations correspond to a TOF of 25 ms and are limited by the maximum observable time during the experiment. Uncertainty bands are obtained by a Monte Carlo method based on the detection angle and trap frequency errors matching the oscillations of the ensemble size. The measurements agree well with the simulation and the coupling of the dynamics in all dimensions allows to extrapolate the behavior in the entire horizontal plane as shown by the purple dashed lines. We find an overall improvement by 3.7 dB in the extrapolated 2D expansion rate energy, when reducing the scattering length. The purple star highlights the minimum 2D energy at $10 a_0$, as prominently featured in the inset.

II. RESULTS

We apply the matter-wave lensing protocol as described in reference [52]. A detailed overview of the experimental setup is provided in section IV A. The atoms are held in a crossed optical dipole trap (ODT) with cycled beam configuration crossing under an angle of 70° . In the following, the $\{x, y, z\}$ -coordinate system refers to the trap frame as defined by the principal axes of the confining potential and used to specify all trap frequencies. We image the $\{x', z\}$ -plane, obtaining the camera frame $\{x', y', z\}$ by rotating around the vertical z -axis by approximately 30° . To implement time-averaged optical potentials [53] we perform a center-position modulation (CPM) along the horizontal axis of the trapping beams, using an acousto-optical modulator (AOM). This approach allows to create harmonic traps with variable width and depth in the horizontal $\{x, y\}$ -plane, but does not feature independent control of the trap frequencies in x - and y -direction or changing the potential shape in z -direction. By rapidly relaxing the trap within 50 μs we cause a sudden reduction in trap frequencies from initial frequencies ω_i^I to final frequencies $\omega_i^F < \omega_i^I$ for $i \in \{x, y\}$, inducing collective mode excitations [54, 55].

Subsequently, the ensemble is collimated by turning off the trapping potential at the turning point of the resulting oscillations of the ensemble size.

We apply this method at two different scattering lengths $158 a_0$ and $10 a_0$ at which the interaction and kinetic energy terms respectively dominate (c.f. section IV D). In the following we differentiate between expansion energies along a singular axis in i -direction (E_i^{1D}), 2D energies in the horizontal plane in which the matter-wave lens is applied (E^{2D}) and the full three dimensional expansion energy (E^{3D}). For both measurements at the two different scattering lengths, we use the same initial and final trap configurations, with small variations of the parameters resulting only from pointing instabilities of the ODT beams which we relate to the time passed between the two measurement campaigns. In both cases the initial trap is realized without any CPM. We find initial trapping frequencies of $2\pi \times \{72, 144, 115\}$ Hz for $158 a_0$ and $2\pi \times \{62, 149, 96\}$ Hz for $10 a_0$. After relaxation our final trap frequencies are $2\pi \times \{23, 36, 126\}$ Hz for $158 a_0$ and $2\pi \times \{24, 38, 129\}$ Hz for $10 a_0$. In parallel the trap depth is maintained by increasing the laser intensity, suppressing atom number loss. Based on time-of-flight (TOF) measurements of the ensemble's expansion,

we determine the expansion energies along the horizontal¹⁸⁶
 (collimated) x' - and vertical (not collimated) z -direction¹⁸⁷
 within the camera frame for different holding times t_{hold} ¹⁸⁸
 after relaxing the trap. At a scattering length of 158 a_0 ¹⁸⁹
 (Fig. 1a) the minimal value in the collimated direction¹⁹⁰
 yields $E_{x'}^{\text{1D}} = (1.00 \pm 0.17) \text{ nK}$ and is achieved after a¹⁹¹
 holding time of 24 ms. For 10 a_0 (Fig. 1b) we find the¹⁹²
 minimum for a holding time of 22 ms after decompression¹⁹³
 resulting in a minimal value of $E_{x'}^{\text{1D}} = (340 \pm 12) \text{ pK}$ ¹⁹⁴
 after up to 25 ms TOF. While the behavior derived from¹⁹⁵
 simulations (c.f. section IV C) agrees with these findings,¹⁹⁶
 for the points below 1 nK a portion of interaction energy¹⁹⁷
 remains and the ensemble has not yet reached the linear¹⁹⁸
 expansion regime at that point. When correcting for this¹⁹⁹
 effect, by simulating for a TOF of 250 ms the asymptotic²⁰⁰
 behavior yields a minimum of $E_{x'}^{\text{1D}} = (429 \pm 56) \text{ pK}$ after²⁰¹
 a holding time of 22.1 ms.²⁰²

The excellent agreement between experiment and simulation allows to understand the ensemble's dynamics²⁰³ in the entire horizontal plane, as both theoretical approaches feature coupling of ensemble oscillations in all directions. Including the axis which cannot be directly observed, we extrapolate the resulting 2D expansion energies as depicted by the dashed purple lines in Fig 1. At 10 a_0 we find a minimal value of $E^{\text{2D}} = (301 \pm 65) \text{ pK}$ for a TOF of 25 ms, which corresponds to an improvement by 3.7 dB over the 158 a_0 case. Extending the simulation to the ballistic regime as before, yields a final value of $E^{\text{2D}} = (438 \pm 77) \text{ pK}$ for 250 ms TOF (c.f. Fig. 2a).²¹⁰

III. DISCUSSION

A. Comparison to previous results

In this work we applied our matter-wave collimation²¹⁸ protocol previously developed for ^{87}Rb to a ^{39}K BEC and²¹⁹ prove the ease of application to another atomic species,²²⁰ demonstrating a reduction of the expansion energy by²²¹ 13 dB compared to the non-collimated case, as given for²²² vanishing holding time. Considering the mass ratio of²²³ both elements, the obtained energy of $(1.00 \pm 0.17) \text{ nK}$ ²²⁴ for ^{39}K at 158 a_0 , corresponding to an expansion velocity of $(0.46 \pm 0.04) \text{ mm/s}$, is comparable to the previously²²⁶ achieved result of $(3.2 \pm 0.6) \text{ nK} \equiv (0.55 \pm 0.05) \text{ mm/s}$ with²²⁷ ^{87}Rb [52] at its natural background scattering length²²⁸ of $\sim 100 \text{ a}_0$ [56]. The remaining difference can be attributed to variations in the trap frequency ratios between the two experiments, rather than to the difference in scattering length, since changing the latter by less than a few multiples does not significantly affect the expansion rate when staying within the strong interaction regime [57, 58]. Hence, the observed outcome aligns with expectations as the technique only depends on the ensemble's dynamics governed by interactions and trap frequencies and accurately described through the Gross-Pitaevskii equation. More importantly, we show that the final expansion energy after the lens can be further reduced.

duced by transitioning into the weak interaction regime, as done here through minimizing the scattering length by means of a magnetic Feshbach resonance. By reducing the repulsive forces driving the expansion after release from the trap, we achieve expansion energies well below 1 nK, which is necessary to match the requirements of proposed experiments, e.g. for, but not limited to, gravitational wave detection [59–64], test of the Weak Equivalence Principle [8, 11, 65] or the search for dark matter [66–68]. While the energies realized here are still an order of magnitude larger than in previous demonstrations in two [47] and three dimensions [48], our method can be applied directly in the ODT. Hence it is suitable for setups and applications which do not allow for an extended pre-expansion time before applying the lens due to constraints regarding experimental cycle time or spatial dimensions. Lower expansion energies are currently limited by the achievable maximum CPM amplitude of 200 μm which in turn restricts the range of accessible trapping frequencies to the values given in section II.

B. Scattering length and trap frequency dependencies

To gain insight into the impact of the scattering length onto the collimation, we analyze the ensemble's behavior in the weak interaction regime by simulating the dynamics with an adapted theoretical model for two different scenarios (Fig. 2a). Starting from trap frequencies of $2\pi \times 60 \text{ Hz}$ in all directions, we apply a common reduction in the horizontal plane while maintaining the frequency along the z -axis, as shown by the theoretical grey lines. For all scenarios we evaluate the optimal holding time after relaxing the trap for minimizing E^{2D} and study the behavior for different squared trap frequency ratios $\alpha_i = (\omega_i^{\text{F}}/\omega_i^{\text{I}})^2$, which would provide the energy scaling in the ideal gas regime [69]. As previously discussed in reference [47] and also observed here, the energy reduction for a BEC is significantly higher due to an interplay of interactions and coupling of the oscillations of the ensemble widths along each axis. From the theory simulations we find a reduction of the expansion energy towards smaller scattering length for $\alpha_x = \alpha_y > 4/9$ as shown by the dashed grey line. This result matches the expected dynamics of an ensemble during free-fall expansion without any lensing and is explained by repulsive interactions after removing the trapping potential [33, 57, 58]. Interestingly, we identify a minimal expansion energy at non-zero interactions for $\alpha_x = \alpha_y \lesssim 4/9$, as depicted by the continuous, dotted and dash-dotted grey lines. These curves clearly show that for smaller values of α_i , reaching optimal energies requires to move towards higher scattering length values. While in these cases minimizing the interaction energy still reduces the corresponding forces upon release, it also reduces the final ensemble width within the trap considerably. Hence, the kinetic energy from the resulting fundamental momentum spread as given by

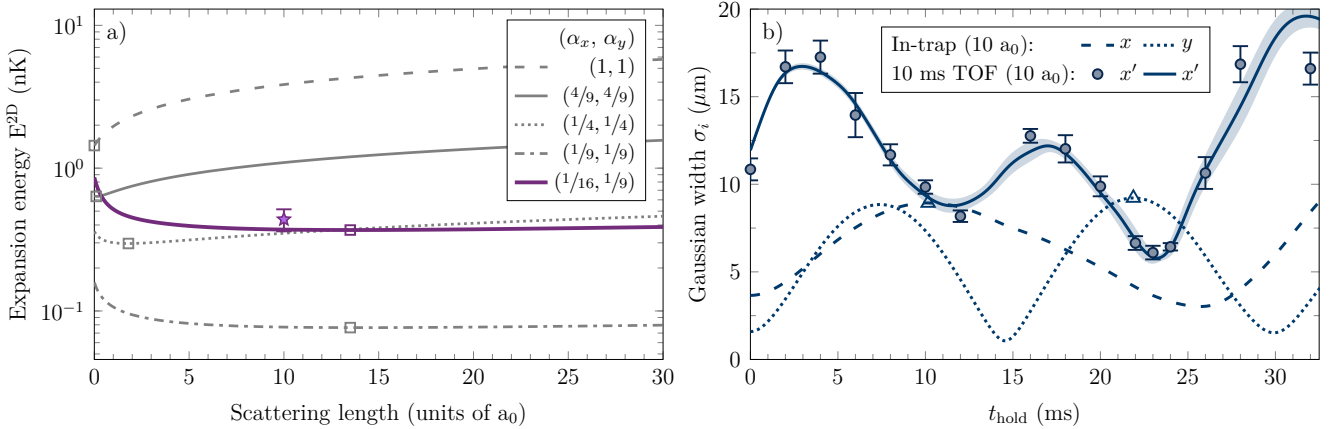


FIG. 2. (a) Simulated 2D expansion energy E^{2D} in the collimated plane for different scaling factors α_i and for the configuration used in the experiment (see section II) after 250 ms TOF. (b) Measured ensemble width in x' -direction for 10 ms TOF at $10 a_0$ and corresponding oscillations of the ensemble widths in x - and y -direction within the trapping potential. For a common frequency reduction along both lensed directions with $\alpha_x = \alpha_y$ taking respectively the values $\{1, 4/9, 1/4, 1/9\}$, the minimal energies are obtained for a scattering length a being respectively $\{0, 0.1, 1.8, 13.5\} a_0$ and identified by the squares for each case. Note, that the sequence becomes more robust against changes of the scattering length with larger frequency reduction, as the minima become more shallow. The purple star resembles the lowest 2D experimental expansion energy presented in Fig. 1b (obtained here for 250 ms TOF). While the curves are simulated for a fixed set of parameters, this point is obtained within a Monte-Carlo simulation including all experimental uncertainties. The error bar denotes 2σ deviation while the central point stands for the mean value (see section IV C). Qualitatively, the experimental configuration closely resembles the case of $\alpha_x = \alpha_y = 1/9$. The resulting expansion energies are globally shifted towards higher values, since $\alpha_x \approx 1/16$ and $\alpha_y \approx 1/9$. This causes the optimal release points to differ for each axis as marked by the triangle symbols in panel 2b, highlighting the importance of a symmetric choice of α -values.

the uncertainty principle increases and the optimal scattering length must be found considering both contributions. To achieve a minimum momentum spread in free fall one hence wants to increase the interactions during the lens to maximize the cloud size and cancel them at the release time. However, given that the interactions are controlled via magnetic fields such an optimization is technically not feasible, as it typically takes tens of millisecond to change the magnetic field [51]. Therefore the optimal scattering length has to be found as a trade-off between the maximum size achievable within the trap and minimal repulsive interactions in free fall along the horizontal direction. Such optimized configurations are highlighted by the empty squares in Fig. 2a. Regarding the experimental setup, as shown by the purple line, where the change in aspect ratio is not the same for both directions, $\alpha_x \approx 1/16$ and $\alpha_y \approx 1/9$, we recover the same behavior as described above for the case $\alpha_x = \alpha_y \lesssim 4/9$, but with globally higher energies. The similarity can be explained by the fact that $\sqrt{\alpha_x \alpha_y} = 1/12$. Note here that the purple star is identical to the one already shown in Fig. 1b.

To get further insight of the complex behavior of the matter wave for different aspect ratios we now compare in Fig 2b the simulated in-trap oscillations in x - and y -direction, respectively presented with dashed and dotted lines, with the observed ensemble width after 10 ms TOF at $a = 10 a_0$. From the experimental measurements (blue

points) we find two distinct minima, each of which can be assigned to the maxima of the underlying ensemble widths within the trap along a different axis (empty blue triangles). In this specific case the lowest expansion energy E^{2D} is found near the optimal collimation of the y -direction, closely resembling the case $\alpha_x = \alpha_y = 1/9$ in Fig. 2a. Compared to the symmetric case the globally higher energies are hence explained by the energy contribution of the other direction, which always exhibits a non-vanishing expansion at release, as long as the aspect ratios are not integer multiples of each other. When performing additional simulations at $a = 30 a_0$, we further note that the optimal release timing is extremely robust with respect to changes of the scattering length, giving only 0.3 ms offset in this particular case. While in practice such changes might arise from technical limitations, e.g. due to imperfect control of the Feshbach field, the offset is fundamentally expected, since changing the repulsive interactions within the trap alters the frequency of the excited oscillations.

Overall, our analysis yields the choice of trapping frequencies to be more important due to their enhanced scaling and the effects of asymmetric expansion compared to the exact scattering length knowledge which is more difficult to pinpoint in practice. Besides allowing to extract the 2D expansion energy from the measurements, the adequacy between the experiment and theory model in Fig. 1 and Fig. 2 allow us in the following to iden-

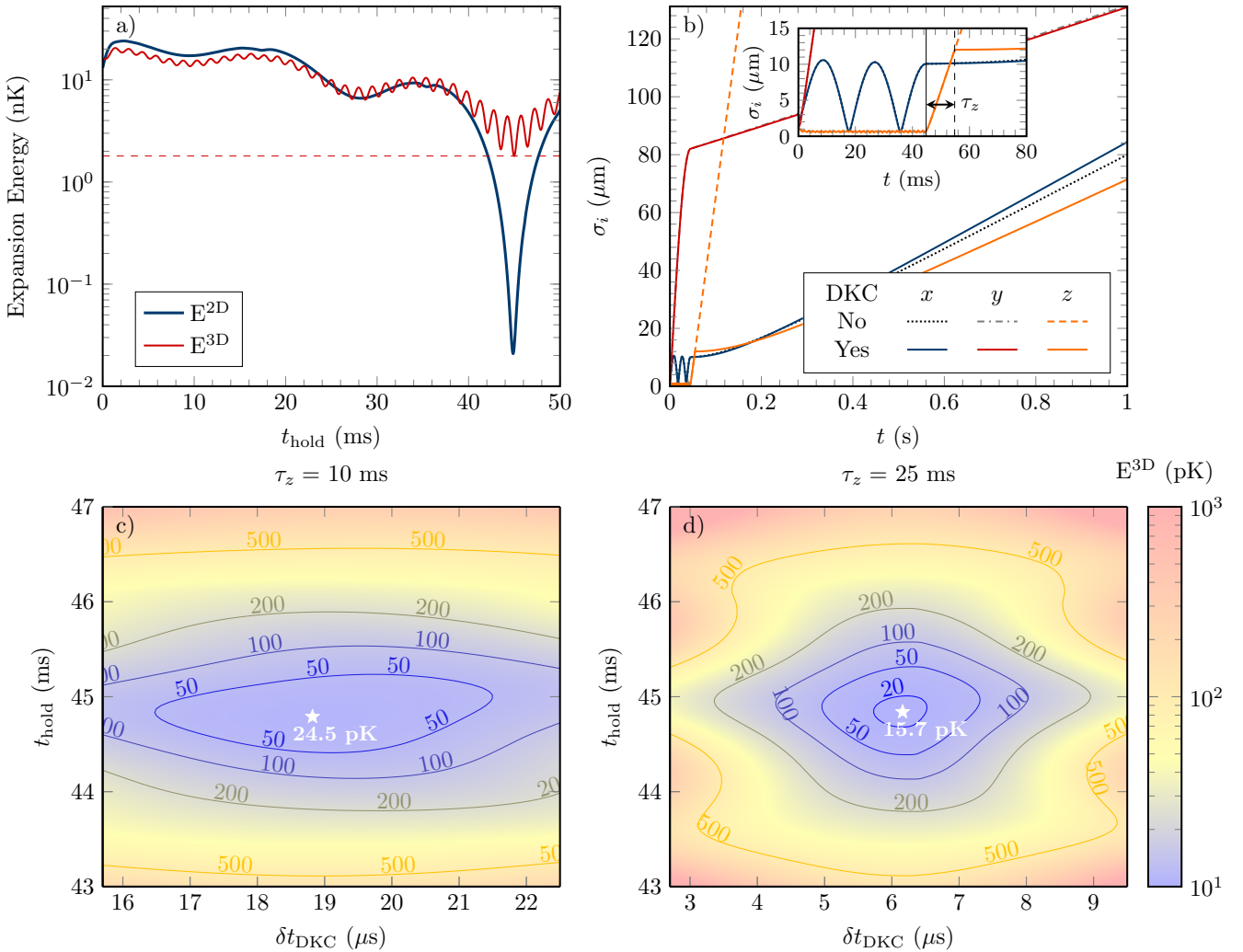


FIG. 3. Generating a delta-kick collimated BEC in the regime of tens of pK. We take advantage of the holding process after trap relaxation to minimize the energy in the $\{x, y\}$ -plane (a) (red line). Subsequently, a short pre-TOF τ_z allows the ensemble to expand, followed by a DKC to collimate the third direction (b). We show the width evolution in all three directions after the optimal holding period without (non-solid lines) and with a DKC (solid lines). The inset shows the dynamics in the trapping potential, highlighting release (solid black line) and DKC (black dashed line) timings. This process leads to a reduced 3D expansion energy expressed as a function of the lensing time and the DKC duration after a pre-TOF of 10 ms (c) and 25 ms (d), leading to respectively 24.5 pK and 15.7 pK.

tify advanced collimation scenarios. Consecutively, we₃₀₉ discuss two 3D collimation sequences based on the com-₃₁₀ bination of a 2D in-trapped collimation combined with₃₁₁ a pulse delta-kick method collimating the third axis to₃₁₂ reach the pK regime [48, 70].

horizontal dashed line in Fig. 3a. To overcome this limitation we consider a short pre-TOF τ_z at the end of the holding process followed by a pulsed DKC protocol [43, 47–49]. We study the theoretically achievable expansion energies for this sequence in an advanced scenario which is specifically tailored towards the capabilities of the improved apparatus as presented in reference [71] and highlight the crucial requirements for the implementation. Instead of a recycled ODT, the setup features two individually controllable beams, each with up to 16 W of optical power at a wavelength of 1064 nm. This configuration allows to realize a variety of possible trap geometries and especially to design common turning points for the oscillations of the ensemble widths along both principal axes. Further-

303 C. Advanced Scenario

304 Since neither the demonstrated method, nor the exper-
305 imental apparatus is designed to collimate the remaining
306 vertical axis, the achievable 3D expansion energies are
307 limited to the nanokelvin regime, regardless of the per-
308 formance in the horizontal plane, as shown by the hori-

more, 2D acousto-optical deflectors (AODs) [*AA Opto-Electronic DTSXY-400-1064*] are used to create time-averaged optical potentials instead of the previously used AOM. In combination with the implemented lens-system, their superior bandwidth allows for CPM amplitudes of at least 1.5 mm and consequently to access lower final trap frequencies and expansion energies. Finally, for the DKC, the second AOD axis is needed to shift the ODT beams vertically and match the position of the atomic cloud for a maximum pre-TOF of $\tau_z = 25$ ms, corresponding to a free-fall distance of 3 mm.

For E^{2D} we numerically find minimal values below 20 pK for a holding time of 42.5 ms switching the trap frequencies from $2\pi \times \{152.7, 310.7, 342.6\}$ Hz to $2\pi \times \{28.1, 5.6, 340.0\}$ Hz at $10 a_0$ scattering length (Fig. 3a). For the final trap configuration 150 mW of optical power at a CPM amplitude of 175 μm for one and 450 mW with 800 μm modulation stroke for the other beam is required. Indeed, as the frequency along the vertical axis is much higher than the two others, the DKC (black dashed line in the inset of Fig. 3b) will not significantly affect the other direction as shown by the black dotted and dash-dotted curves in Fig. 3b. For an easy configuration with only $\tau_z = 10$ ms pre-TOF, corresponding to a free fall distance of 490 μm , experimentally accessible in practice, we obtain a minimal 3D expansion energy of $E^{3D} = 24.5$ pK with a $\delta t_{DKC} = 18.8$ μs long delta-kick pulse and 44.8 ms of lensing as shown in Fig. 3c and optimised using a simulated annealing algorithm [72]. Moreover, the implementation is expected to be robust against variations of the experimental parameters as it allows to achieve energies below 50 pK for a wide range of holding and delta-kick durations. Naturally, even better performance can be obtained by increasing the pre-TOF duration at the expense of the overall robustness with respect to the delta-kick timing [43]. For $\tau_z = 25$ ms of pre-TOF, we find final energies as low as $E^{3D} = 15.7$ pK, but requiring a DKC of only $\delta t_{DKC} = 6.2$ μs (Fig. 3d). The simulation explicitly takes the AOD's response time of 3 μs into account, as it is on the same order of magnitude as δt_{DKC} . While other experimental limitation e.g. due to the bandwidth of the different control loops may apply, the AOD is the slowest component involved and therefore poses the relevant limitation for the advanced scenario, contrary to the measurements in Fig. 1. Nevertheless, such timings can be experimentally challenging when being limited to the center-position modulation frequency below 100 kHz as relevant time scale or using rf-switches with switching times of several μs . For such short signals arbitrary waveform generators based on direct digital synthesizers (DDS) with a high sampling rate offer a convincing solution. In this case we use a software defined radio [*Ettus USRP X310*], whose DDS allows to interrupt the waveform at any given sample and match the pulse length with a resolution of 50 ns for a typical sampling rate of 20 MHz. As before using a low scattering length assists in the overall collimation. However, simulating the same sequence for a scattering length of $158 a_0$ in particular,

still leads to expansion energies of $E^{3D} = 97.5$ pK for $\tau_z = 10$ ms of pre-TOF and $E^{3D} = 81.9$ pK for 25 ms pre-TOF with 17.6 μs and 7.1 μs long delta-kick pulses, respectively.

Hence, the analyzed two-step process opens up the path to approach ($a = 158 a_0$) and even exceed ($a = 10 a_0$) the results that were obtained in a drop-tower [48], on the International Space Station [49] and within a long-baseline device [47]. Combining these results with a strategy for rapid evaporation [71] and a bright source for fast MOT loading [73], compact or even field-deployable devices can reach experimental repetition rates higher than 0.5 Hz with BECs consisting of 3×10^5 atoms and state-of-the-art collimation.

IV. METHODS

A. Experimental apparatus

We use the same setup as for the previous matter-wave lens study with ^{87}Rb [52], featuring a crossed ODT in recycled beam configuration (Fig. 4). A detailed description of the vacuum, laser and coil systems used can be found in references [8, 10, 74]. The ODT is based on a 1960 nm fiber laser [*IPG TLR-50-1960-LP*] which is intensity stabilized by a feedback loop, controlling a linearized Pockels cell. The crossed trap is realized by recycling the same beam, passing the atoms again under an angle of 70° . We ensure orthogonal beam polarization to avoid running lattice formation. Due to the elliptical beam shape of the fiber laser output we obtain different beam waists of 30 μm in horizontal and 45 μm in vertical direction. Taking losses at all optical elements into account, the maximal power which can be delivered to the atoms is limited to 8 W for the initial and 6 W for the recycled beam. A custom-made AOM [*Polytec ATM-1002FA53.24*] is used to implement time-averaged optical potentials of harmonic shape along one beam axis [53, 75]. It is further utilized to control the beam power at the lower end of the intensity stabilization. By focusing the beam onto the atomic cloud, the change in deflection angle of the AOM is translated into a parallel displacement of the beam. For the initial beam, the bandwidth of the AOM allows for a maximum CPM amplitude of 200 μm . For the recycled beam, the same configuration corresponds to a CPM amplitude of 300 μm due to the additional re-collimation and re-focusing, and the increased path length in-between. Due to the experimental configuration, the recycled beam is fully determined by the state of the initial beam and hence the setup does not allow to choose the trap frequencies in x - and y -direction independently. The required frequency modulation of the rf-signal driving the AOM is generated with a combination of voltage controlled oscillator [*Mini-Circuits ZOS-150+*] to provide the actual signal and an arbitrary waveform generator [*Rigol DG1022Z*], which provides the waveform. For the whole experimen-

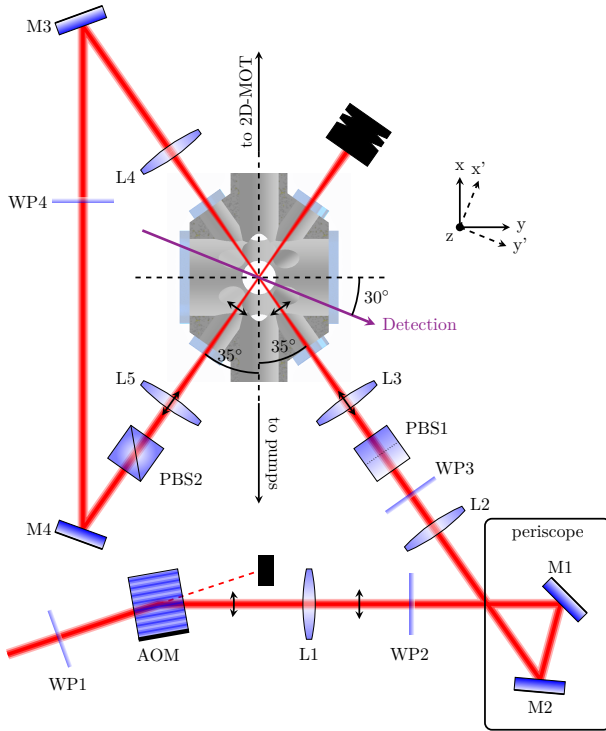


FIG. 4. Experimental apparatus to create the optical dipole trap and the matter-wave lens. A three-lens system (L_1, L_2, L_3) with focal lengths $f_1 = 100\text{ mm}$, $f_2 = 300\text{ mm}$ and $f_3 = 150\text{ mm}$ translates the change in AOM deflection angle into a parallel displacement, while simultaneously focusing the beam to a waist of 30 (45) μm in horizontal (vertical) direction. Orthogonal polarization between the crossing beams is realized by a combination of $\lambda/2$ -wave plates (WP3 and WP4) and polarizing beam splitters (PBS1 and PBS2). For perfect alignment and equal beam power the trap frame $\{x, y, z\}$, as given by the principal axes of the optical potential, resembles the symmetry axes of the vacuum chamber. The camera frame $\{x', y', z\}$ is obtained by a rotation around the z -axis, with the exact detection angle depending on the beam configuration and alignment. The figure is taken from reference [52] and was published under Creative Commons Attribution 4.0 International License. Here the orientation of the detection arrow and the naming of the coordinate systems was altered to account for changes of the apparatus compared to the source material.

the related camera frame $\{x', y', z\}$ can be obtained from the trap frame $\{x, y, z\}$ by rotating clockwise around the z -axis by an angle of $\sim 30^\circ$. Note, that the exact angle depends on the beam configuration prior to detection due to the resulting rotation of the trap frame.

B. Ensemble preparation

We apply a trap loading and state preparation sequence optimized for ^{39}K as described in reference [74]. We load a 3D-magneto optical trap on the D_2 -line from a 2D-MOT, trapping 1×10^9 atoms within 4 s. Subsequently, we apply a hybrid D_1 - D_2 compression MOT to increase the ensemble's density and grey molasses cooling on the D_1 -line for cooling the ensemble to sub-Doppler temperatures [76]. In this manner we prepare 4×10^8 atoms at a temperature of $12\text{ }\mu\text{K}$ within 56 ms after turning off the 2D-MOT. For loading the ODT we use a center-position modulation amplitude of $160\text{ }\mu\text{m}$ to improve the mode matching of the crossing region with the cloud, transferring 12×10^6 atoms into the $54\text{ }\mu\text{K}$ deep ODT, with a temperature of $8.5\text{ }\mu\text{K}$. Afterwards, we prepare the ensemble in $|F = 1, m_F = -1\rangle$ with a multi-loop state preparation scheme based on microwave adiabatic rapid passages. This allows to use the broad Feshbach resonance at 32.6 G [77] to adjust the scattering length to positive values, necessary for direct evaporative cooling [78]. We use the evaporation sequence optimized for the largest number of condensed particle, rather than the shortest experimental cycle time with the highest atomic flux, realizing a quasi-pure BEC of up to 2×10^5 atoms after 3.9 s of evaporative cooling at a scattering length of $158\text{ }a_0$. For the measurement at $158\text{ }a_0$ we perform the matter-wave lens 100 ms after creating the BEC by increasing the center-position modulation amplitude to the achievable maximum, as stated before. For the measurement at $10\text{ }a_0$, we additionally adiabatically sweep the magnetic field towards the broad minimum between the resonance at 32.6 G and the next higher one at 162.8 G after creating the BEC and before performing the matter-wave lens.

C. Data acquisition and analysis

We perform TOF measurements for different holding times after relaxing the trap with a total experimental cycle time of 12 s. Subsequently we describe the obtained density profile either by a Gaussian or a Thomas-Fermi distribution, depending on the scattering length used. For the measurements at $158\text{ }a_0$ the Thomas-Fermi radii $R_i(t)$ are transformed into their equivalent standard deviation $\sigma_i(t)$ using $\sigma_i(t) = R_i(t)/\sqrt{7}$ [39, 70]. Individual data points are taken for a holding time spacing of 1 ms and a TOF spacing of 5 ms. Each measurement is repeated at least four times. At $10\text{ }a_0$ we fit a Gaussian to the obtained density distribution. For

tal sequence a constant modulation frequency of 20 kHz is used, which is sufficiently large compared to any occurring trap frequency. We define the trap frame $\{x, y, z\}$ as the principal axes of the trapping potential, given by the eigenvectors of the curvature in the critical point. In the case of equal ODT beams in terms of power and waist it resembles the symmetry axis of the experimental setup as shown in Fig. 4, while any deviations from the ideal beam configuration result in rotations of the coordinate system around the z -axis. Finally, detection is performed by absorption imaging with unity magnification. The camera is situated in the $\{x, y\}$ -plane and

these measurements the TOF spacing is reduced to 1 ms at the expense of the holding time spacing which is increased to at least 2 ms, in order to obtain better statistics for the extracted ensemble expansion. For each individual dataset, measurements are performed over the course of 12 hours of continuous operation. With this approach we ensure comparability within each dataset and avoid trap frequency drifts caused by thermal effects from power cycling the 1960 nm laser in between measurement days. To obtain the linear expansion rate for a given holding time, we only consider the data taken for more than 10 ms TOF, avoiding the resolution limitation of our detection system. Finally, the fitted expansion rates v_i are transformed into 1D expansion energy using $E_i^{1D} = k_B T_i / 2 = m v_i^2 / 2$.

To simulate the behavior of the ensemble, we determine the trapping frequencies by fitting the oscillations of the ensemble width with respect to the holding time for a constant TOF in the trap frame and by projecting them into the rotated camera frame, afterwards. Since the detection angle relative to the trap frame changes with respect to small deviations of the ODT beam alignment, the exact angle is evaluated for each measurement separately and fitted to the data, as well. We optimize the fit parameters on five different TOF in between 10 and 25 ms simultaneously with equal weighting, obtaining a single set of values, which provide the overall smallest error. Based on the frequencies found, we perform simulations of the ensemble's behavior using the two approaches provided in section IV D. The error bands stem from 1000 Monte-Carlo simulations within the obtained errors of trap frequencies, detection angle and scattering length (at 10 a_0) as determined by fitting the ensemble width and the magnetic field characterization of the apparatus.

For the advanced scenario we take experimental parameters and technical limitations of the setup, e.g. the rise time of the AOD, into account. We search for optimal 3D collimation by simulating a grid with a step size of 36 μs for the lensing and 62 ns for the DKC, using a simulated annealing algorithm [72] for the absolute minimum in each case.

D. Theoretical model

For a scattering length of 158 a_0 , the interaction energy exceeds the kinetic energy of the ensemble, so the BEC dynamics is well described by the scaling equations of Refs. [79, 80]

$$\ddot{\lambda}_i(t) + \omega_i^2(t)\lambda_i(t) = \frac{\omega_i^2(0)}{\lambda_i \lambda_x \lambda_y \lambda_z}, \quad (1)$$

where the dimensionless variable $\lambda_i(t) = R_i(t)/R_i(0)$ characterizes the evolution of the size of the condensate in the direction $i \in \{x, y, z\}$. In this expression, $R_i(t)$ is the Thomas-Fermi radius in the direction i , and the initial radius is given by [81]

$$R_i(0) = a_{\text{osc}} \frac{\bar{\omega}(0)}{\omega_i(0)} \left(\frac{15Na}{a_{\text{osc}}} \right)^{1/5}, \quad (2)$$

with the average length of the quantum harmonic oscillator $a_{\text{osc}} = [\hbar/m\bar{\omega}(0)]^{1/2}$ and the geometric mean of the initial trapping frequencies $\bar{\omega}(0) = [\omega_x(0)\omega_y(0)\omega_z(0)]^{1/3}$. From the solution of Eq. (1) we extract the standard deviations $\sigma_i(t) = R_i(t)/\sqrt{7}$ associated with the atomic density, that we compare with the experimental measurements obtained as described in section IV C.

In the case of a scattering length of 10 a_0 , the Thomas-Fermi approximation is no longer suitable to accurately describe the dynamics of the BEC. Instead, we follow a variational approach and describe the BEC with a Gaussian ansatz [82, 83]. This leads in a harmonic trap to the following set of coupled differential equations

$$\ddot{\sigma}_i(t) + \omega_i^2(t)\sigma_i(t) = \frac{\hbar^2}{4m^2\sigma_i^3(t)} + \frac{\hbar^2aN}{4\sqrt{\pi}m^2} \frac{1}{\sigma_i\sigma_x\sigma_y\sigma_z}, \quad (3)$$

for the standard deviations $\sigma_i(t)$ of the atomic density. The time-independent version of Eq. (3) is used to determine the initial size $\sigma_i(0)$ of the ensemble, which converges to the oscillator length for vanishing scattering length.

DATA AVAILABILITY

The data used in this manuscript is available from the corresponding author upon reasonable request.

-
- [1] C. L. Degen, F. Reinhard, and P. Cappellaro, Quantum sensing, Rev. Mod. Phys. **89**, 035002 (2017).
 - [2] O. Mandel, M. Greiner, A. Widera, T. Rom, T. W. Hänsch, and I. Bloch, Controlled collisions for multi-particle entanglement of optically trapped atoms, Nature **425**, 937 (2003).
 - [3] I. M. Georgescu, S. Ashhab, and F. Nori, Quantum simulation, Rev. Mod. Phys. **86**, 153 (2014).
 - [4] M. Kasevich and S. Chu, Atomic interferometry using stimulated raman transitions, Phys. Rev. Lett. **67**, 181 (1991).
 - [5] M. Kasevich and S. Chu, Measurement of the gravitational acceleration of an atom with a light-pulse atom interferometer, Applied Physics B **54**, 321 (1992).
 - [6] F. Riehle, T. Kisters, A. Witte, J. Helmcke, and C. J. Bordé, Optical ramsey spectroscopy in a rotating frame:

- 589 Sagnac effect in a matter-wave interferometer, Phys. Rev. Lett. **67**, 177 (1991).
 590 653
 591 [7] A. D. Cronin, J. Schmiedmayer, and D. E. Pritchard, Optics and interferometry with atoms and molecules, Rev. Mod. Phys. **81**, 1051 (2009).
 592 655
 593 [8] D. Schlippert, J. Hartwig, H. Albers, L. L. Richardson, C. Schubert, A. Roura, W. P. Schleich, W. Ertmer, and E. M. Rasel, Quantum test of the universality of free fall, Phys. Rev. Lett. **112**, 203002 (2014).
 594 658
 595 [9] M. G. Tarallo, T. Mazzoni, N. Poli, D. V. Sutyrin, X. Zhang, and G. M. Tino, Test of einstein equivalence principle for 0-spin and half-integer-spin atoms: Search for spin-gravity coupling effects, Phys. Rev. Lett. **113**, 023005 (2014).
 596 661
 597 [10] H. Albers, A. Herbst, L. L. Richardson, H. Heine, D. Nath, J. Hartwig, C. Schubert, C. Vogt, M. Woltmann, C. Lämmerzahl, S. Herrmann, W. Ertmer, E. M. Rasel, and D. Schlippert, Quantum test of the universality of free fall using rubidium and potassium, The European Physical Journal D **74**, 10.1140/epjd/e2020-10132-6 (2020).
 600 664
 601 [11] P. Asenbaum, C. Overstreet, M. Kim, J. Curti, and M. A. Kasevich, Atom-interferometric test of the equivalence principle at the 10^{-12} level, Phys. Rev. Lett. **125**, 191101 (2020).
 604 667
 605 [12] M. Carlesso, S. Donadi, L. Ferialdi, M. Paternostro, H. Ulbricht, and A. Bassi, Present status and future challenges of non-interferometric tests of collapse models, Nature Physics **18**, 243 (2022).
 608 670
 609 [13] T. Kovachy, P. Asenbaum, C. Overstreet, C. A. Donnelly, S. M. Dickerson, A. Sugarbaker, J. M. Hogan, and M. A. Kasevich, Quantum superposition at the half-metre scale, Nature **528**, 530 (2015).
 612 673
 613 [14] A. Bassi, K. Lochan, S. Satin, T. P. Singh, and H. Ulbricht, Models of wave-function collapse, underlying theories, and experimental tests, Rev. Mod. Phys. **85**, 471 (2013).
 616 676
 617 [15] B. Schrinski, P. Haslinger, J. Schmiedmayer, K. Hornberger, and S. Nimmrichter, Testing collapse models with bose-einstein-condensate interferometry, Phys. Rev. A **107**, 043320 (2023).
 620 680
 621 [16] G. Rosi, F. Sorrentino, L. Cacciapuoti, M. Prevedelli, and G. M. Tino, Precision measurement of the newtonian gravitational constant using cold atoms, Nature **510**, 518 (2014).
 624 683
 625 [17] R. H. Parker, C. Yu, W. Zhong, B. Estey, and H. Müller, Measurement of the fine-structure constant as a test of the standard model, Science **360**, 191 (2018).
 628 686
 629 [18] L. Morel, Z. Yao, P. Cladé, and S. Guellati-Khélifa, Determination of the fine-structure constant with an accuracy of 81 parts per trillion, Nature **588**, 61 (2020).
 633 690
 634 [19] T. L. Gustavson, P. Bouyer, and M. A. Kasevich, Precision rotation measurements with an atom interferometer gyroscope, Physical Review Letters **78**, 2046 (1997).
 638 693
 639 [20] B. Canuel, F. Leduc, D. Holleville, A. Gauguet, J. Fils, A. Virdis, A. Clairon, N. Dimarcq, C. J. Bordé, A. Landragin, and P. Bouyer, Six-axis inertial sensor using cold-atom interferometry, Phys. Rev. Lett. **97**, 010402 (2006).
 643 696
 644 [21] S. M. Dickerson, J. M. Hogan, A. Sugarbaker, D. M. S. Johnson, and M. A. Kasevich, Multiaxis inertial sensing with long-time point source atom interferometry, Phys. Rev. Lett. **111**, 083001 (2013).
 648 699
 649 [22] I. Dutta, D. Savoie, B. Fang, B. Venon, C. Garrido Alzar, R. Geiger, and A. Landragin, Continuous cold-atom iner-
 653
 656 tial sensor with 1 nrad/sec rotation stability, Phys. Rev. Lett. **116**, 183003 (2016).
 658 [23] D. Savoie, M. Altorio, B. Fang, L. A. Sidorenkov, R. Geiger, and A. Landragin, Interleaved atom interferometry for high-sensitivity inertial measurements, Science advances **4**, eaau7948 (2018).
 661 [24] J. Le Gouët, T. E. Mehlstäubler, J. Kim, S. Merlet, A. Clairon, A. Landragin, and F. Pereira dos Santos, Limits to the sensitivity of a low noise compact atomic gravimeter, Applied Physics B **92**, 133 (2008).
 664 [25] Z.-K. Hu, B.-L. Sun, X.-C. Duan, M.-K. Zhou, L.-L. Chen, S. Zhan, Q.-Z. Zhang, and J. Luo, Demonstration of an ultrahigh-sensitivity atom-interferometry absolute gravimeter, Phys. Rev. A **88**, 043610 (2013).
 667 [26] V. Ménoret, P. Vermeulen, N. Le Moigne, S. Bonvalot, P. Bouyer, A. Landragin, and B. Desruelle, Gravity measurements below 10^{-9} g with a transportable absolute quantum gravimeter, Scientific reports **8**, 12300 (2018).
 670 [27] A. Louchet-Chauvet, T. Farah, Q. Bodart, A. Clairon, A. Landragin, S. Merlet, and F. P. D. Santos, The influence of transverse motion within an atomic gravimeter, New Journal of Physics **13**, 065025 (2011).
 673 [28] V. Schkolnik, B. Leykauf, M. Hauth, C. Freier, and A. Peters, The effect of wavefront aberrations in atom interferometry, Applied Physics B **120**, 311 (2015).
 676 [29] M. Anderson, J. Ensher, M. Matthews, C. Wieman, and E. Cornell, Observation of Bose-Einstein Condensation in a Dilute Atomic Vapor, Science **269**, 198 (1995).
 679 [30] K. B. Davis, M.-O. Mewes, M. A. Joffe, M. R. Andrews, and W. Ketterle, Evaporative cooling of sodium atoms, Physical Review Letters **74**, 5202 (1995).
 682 [31] D. Schlippert, C. Meiners, R. Rengelink, C. Schubert, D. Tell, É. Wodey, K. Zipfel, W. Ertmer, and E. Rasel, Matter-wave interferometry for inertial sensing and tests of fundamental physics, in *CPT and Lorentz Symmetry* (WORLD SCIENTIFIC, 2021).
 685 [32] T. Hensel, S. Loriani, C. Schubert, F. Fitzek, S. Abend, H. Ahlers, J.-N. Siemß, K. Hammerer, E. M. Rasel, and N. Gaaloul, Inertial sensing with quantum gases: a comparative performance study of condensed versus thermal sources for atom interferometry, The European Physical Journal D **75**, 10.1140/epjd/s10053-021-00069-9 (2021).
 688 [33] T. Weber, J. Herbig, M. Mark, H.-C. Nägerl, and R. Grimm, Bose-einstein condensation of cesium, Science (New York, N.Y.) **299**, 232 (2003).
 691 [34] K. S. Hardman, P. J. Everitt, G. D. McDonald, P. Manju, P. B. Wigley, M. A. Sooriyabandara, C. C. N. Kuhn, J. E. Debs, J. D. Close, and N. P. Robins, Simultaneous precision gravimetry and magnetic gradiometry with a bose-einstein condensate: A high precision, quantum sensor, Phys. Rev. Lett. **117**, 138501 (2016).
 694 [35] D. Gochnauer, T. Rahman, A. Wirth-Singh, and S. Gupta, Interferometry in an atomic fountain with ytterbium bose-einstein condensates, Atoms **9**, 58 (2021).
 697 [36] D. N. Aguilera, H. Ahlers, B. Battelier, A. Bawamia, A. Bertoldi, R. Bondarescu, K. Bongs, P. Bouyer, C. Braxmaier, L. Cacciapuoti, C. Chaloner, M. Chwalla, W. Ertmer, M. Franz, N. Gaaloul, M. Gehler, D. Gerardi, L. Gesa, N. Gürlebeck, J. Hartwig, M. Hauth, O. Hellmig, W. Herr, S. Herrmann, A. Heske, A. Hinton, P. Ireland, P. Jetzer, U. Johann, M. Krutzik, A. Kubelka, C. Lämmerzahl, A. Landragin, I. Lloro, D. Massonet, I. Mateos, A. Milke, M. Nofrarias, M. Oswald, A. Pe-

- ters, K. Posso-Trujillo, E. Rasel, E. Rocco, A. Roura,⁷⁷⁹
J. Rudolph, W. Schleich, C. Schubert, T. Schuldt, S. Sei⁷⁸⁰
del, K. Sengstock, C. F. Sopuerta, F. Sorrentino, D. Sum⁷⁸¹
mers, G. M. Tino, C. Trenkel, N. Uzunoglu, W. von Klitz⁷⁸²
ing, R. Walser, T. Wendrich, A. Wenzlawski, P. Weßels,⁷⁸³
A. Wicht, E. Wille, M. Williams, P. Windpassinger, and⁷⁸⁴
N. Zahzam, Ste-quest—test of the universality of free fall⁷⁸⁵
using cold atom interferometry, *Classical and Quantum⁷⁸⁶*
Gravity **31**, 115010 (2014). ⁷⁸⁷
- [37] A. Trimeche, B. Battelier, D. Becker, A. Bertoldi,⁷⁸⁸
P. Bouyer, C. Braxmaier, E. Charron, R. Corgier,⁷⁸⁹
M. Cornelius, K. Douch, N. Gaaloul, S. Herrmann,⁷⁹⁰
J. Müller, E. Rasel, C. Schubert, H. Wu, and F. Pereira⁷⁹¹
dos Santos, Concept study and preliminary design of a⁷⁹²
cold atom interferometer for space gravity gradiometry,⁷⁹³
Classical and Quantum Gravity **36**, 215004 (2019). ⁷⁹⁴
- [38] S. Loriani, D. Schlippert, C. Schubert, S. Abend,⁷⁹⁵
H. Ahlers, W. Ertmer, J. Rudolph, J. M. Hogan, M. A.⁷⁹⁶
Kasevich, E. M. Rasel, and N. Gaaloul, Atomic source se-⁷⁹⁷
lection in space-borne gravitational wave detection, *New⁷⁹⁸*
Journal of Physics **21**, 063030 (2019). ⁷⁹⁹
- [39] R. Corgier, S. Loriani, H. Ahlers, K. Posso-Trujillo,⁸⁰⁰
C. Schubert, E. M. Rasel, E. Charron, and N. Gaaloul,⁸⁰¹
Interacting quantum mixtures for precision atom inter-⁸⁰²
ferometry, *New Journal of Physics* **22**, 123008 (2020). ⁸⁰³
- [40] C. Struckmann, R. Corgier, S. Loriani, G. Kleinsteenberg,⁸⁰⁴
N. Gox, E. Giese, G. Métris, N. Gaaloul, and P. Wolf,⁸⁰⁵
Platform and environment requirements of a satellite⁸⁰⁶
quantum test of the weak equivalence principle at the⁸⁰⁷
\$10^{-17\\$ level (2023), 2310.04212. ⁸⁰⁸
- [41] A. E. Leanhardt, T. A. Pasquini, M. Saba, A. Schirotzek,⁸⁰⁹
Y. Shin, D. Kielpinski, D. E. Pritchard, and W. Ketterle,⁸¹⁰
Cooling bose-einstein condensates below 500 picokelvin,⁸¹¹
Science (New York, N.Y.) **301**, 1513 (2003). ⁸¹²
- [42] P. Medley, D. M. Weld, H. Miyake, D. E. Pritchard, and⁸¹³
W. Ketterle, Spin gradient demagnetization cooling of⁸¹⁴
ultracold atoms, *Phys. Rev. Lett.* **106**, 195301 (2011). ⁸¹⁵
- [43] H. Ammann and N. Christensen, Delta kick cooling: A⁸¹⁶
new method for cooling atoms, *Phys. Rev. Lett.* **78**, 2088⁸¹⁷
(1997). ⁸¹⁸
- [44] J. G. Kalnins, J. M. Amini, and H. Gould, Focusing⁸¹⁹
fountain of neutral cesium atoms with an electrostatic⁸²⁰
lens triplet, *Phys. Rev. A* **72**, 043406 (2005). ⁸²¹
- [45] H. Müntinga, H. Ahlers, M. Krutzik, A. Wenzlawski,⁸²²
S. Arnold, D. Becker, K. Bongs, H. Dittus, H. Duncker,⁸²³
N. Gaaloul, C. Gherasim, E. Giese, C. Grzeschik, T. W.⁸²⁴
Hänsch, O. Hellmig, W. Herr, S. Herrmann, E. Kajari,⁸²⁵
S. Kleinert, C. Lämmerzahl, W. Lewoczko-Adamczyk,⁸²⁶
J. Malcolm, N. Meyer, R. Nolte, A. Peters, M. Popp,⁸²⁷
J. Reichel, A. Roura, J. Rudolph, M. Schiemangk,⁸²⁸
M. Schneider, S. T. Seidel, K. Sengstock, V. Tamma,⁸²⁹
T. Valenzuela, A. Vogel, R. Walser, T. Wendrich,⁸³⁰
P. Windpassinger, W. Zeller, T. van Zoest, W. Ertmer,⁸³¹
W. P. Schleich, and E. M. Rasel, Interferometry with⁸³²
bose-einstein condensates in microgravity, *Phys. Rev.⁸³³*
Lett. **110**, 093602 (2013). ⁸³⁴
- [46] W. Ketterle, D. S. Durfee, and D. M. Stamper-Kurn,⁸³⁵
Making, probing and understanding bose-einstein con-⁸³⁶
densates (1999), arXiv:cond-mat/9904034 [cond-mat]. ⁸³⁷
- [47] T. Kovachy, J. M. Hogan, A. Sugarbaker, S. M. Dicker-⁸³⁸
son, C. A. Donnelly, C. Overstreet, and M. A. Kasevich,⁸³⁹
Matter wave lensing to picokelvin temperatures, *Phys.⁸⁴⁰*
Rev. Lett. **114**, 143004 (2015). ⁸⁴¹
- [48] C. Deppner, W. Herr, M. Cornelius, P. Stromberger,⁸⁴²
T. Sternke, C. Grzeschik, A. Grote, J. Rudolph, S. Her-⁸⁴³
mann, M. Krutzik, A. Wenzlawski, R. Corgier, E. Char-⁸⁴⁴
ron, D. Guéry-Odelin, N. Gaaloul, C. Lämmerzahl,⁸⁴⁵
A. Peters, P. Windpassinger, and E. M. Rasel, Collective-⁸⁴⁶
mode enhanced matter-wave optics, *Phys. Rev. Lett.*
127, 100401 (2021).
- [49] N. Gaaloul, M. Meister, R. Corgier, A. Pichery,⁸⁴⁷
P. Boegel, W. Herr, H. Ahlers, E. Charron, J. R.⁸⁴⁸
Williams, R. J. Thompson, W. P. Schleich, E. M. Rasel,⁸⁴⁹
and N. P. Bigelow, A space-based quantum gas labora-⁸⁵⁰
tory at picokelvin energy scales, *Nature communications*
13, 7889 (2022).
- [50] S. Inouye, M. R. Andrews, J. Stenger, H.-J. Miesner,⁸⁵¹
D. M. Stamper-Kurn, and W. Ketterle, Observation of⁸⁵²
feshbach resonances in a bose-einstein condensate, *Nature*
392, 151 (1998).
- [51] L. Masi, T. Petrucciani, A. Burchianti, C. Fort, M. In-⁸⁵³
guscio, L. Marconi, G. Modugno, N. Preti, D. Trypoge-⁸⁵⁴
orgos, M. Fattori, and F. Minardi, Multimode trapped⁸⁵⁵
interferometer with noninteracting bose-einstein condens-⁸⁵⁶
ates, *Phys. Rev. Research* **3**, 043188 (2021).
- [52] H. Albers, R. Corgier, A. Herbst, A. Rajagopalan,⁸⁵⁷
C. Schubert, C. Vogt, M. Woltmann, C. Lämmerzahl,⁸⁵⁸
S. Herrmann, E. Charron, W. Ertmer, E. M. Rasel,⁸⁵⁹
N. Gaaloul, and D. Schlippert, All-optical matter-wave⁸⁶⁰
lens using time-averaged potentials, *Communications⁸⁶¹*
Physics **5**, 60 (2022).
- [53] R. Roy, A. Green, R. Bowler, and S. Gupta, Rapid cool-⁸⁶²
ing to quantum degeneracy in dynamically shaped atom⁸⁶³
traps, *Phys. Rev. A* **93**, 043403 (2016).
- [54] D. S. Jin, J. R. Ensher, M. R. Matthews, C. E. Wie-⁸⁶⁴
man, and E. A. Cornell, Collective excitations of a bose-⁸⁶⁵
einstein condensate in a dilute gas, *Phys. Rev. Lett.* **77**,⁸⁶⁶
420 (1996).
- [55] M.-O. Mewes, M. R. Andrews, N. J. van Druten, D. M.⁸⁶⁷
Kurn, D. S. Durfee, C. G. Townsend, and W. Ketterle,⁸⁶⁸
Collective excitations of a bose-einstein condensate in a⁸⁶⁹
magnetic trap, *Phys. Rev. Lett.* **77**, 988 (1996).
- [56] M. Egorov, B. Opanchuk, P. Drummond, B. V. Hall,⁸⁷⁰
P. Hannaford, and A. I. Sidorov, Measurement of *s*-wave⁸⁷¹
scattering lengths in a two-component bose-einstein con-⁸⁷²
densate, *Phys. Rev. A* **87**, 053614 (2013).
- [57] T. Kraemer, J. Herbig, M. Mark, T. Weber, C. Chin,⁸⁷³
H.-C. Nägerl, and R. Grimm, Optimized production of a⁸⁷⁴
cesium bose-einstein condensate, *Applied Physics B* **79**,⁸⁷⁵
1013 (2004).
- [58] G. Roati, M. Zaccanti, C. D'Errico, J. Catani, M. Mod-⁸⁷⁶
ugno, A. Simoni, M. Inguscio, and G. Modugno, ³⁹K⁸⁷⁷
bose-einstein condensate with tunable interactions, *Phys.⁸⁷⁸*
Rev. Lett. **99**, 010403 (2007).
- [59] J. M. Hogan, D. M. S. Johnson, S. Dickerson, T. Ko-⁸⁷⁹
vachy, A. Sugarbaker, S.-w. Chiow, P. W. Graham, M. A.⁸⁸⁰
Kasevich, B. Saif, S. Rajendran, P. Bouyer, B. D. Seery,⁸⁸¹
L. Feinberg, and R. Keski-Kuha, An atomic gravitational⁸⁸²
wave interferometric sensor in low earth orbit (agis-leo),⁸⁸³
General Relativity and Gravitation **43**, 1953 (2011).
- [60] B. Canuel, A. Bertoldi, L. Amand, E. Di Pozzo Borgo,⁸⁸⁴
T. Chantrait, C. Danquigny, M. Dovale Álvarez, B. Fang,⁸⁸⁵
A. Freise, R. Geiger, J. Gillot, S. Henry, J. Hinderer,⁸⁸⁶
D. Holleville, J. Junca, G. Lefèvre, M. Merzougui, N. Mi-⁸⁸⁷
elec, T. Monfret, S. Pelisson, M. Prevedelli, S. Reynaud,⁸⁸⁸
I. Riou, Y. Rogister, S. Rosat, E. Cormier, A. Landragin,⁸⁸⁹

- 842 W. Chaibi, S. Gaffet, and P. Bouyer, Exploring gravity⁹⁰⁶
 843 with the migal large scale atom interferometer, Scientific⁹⁰⁷
 844 reports **8**, 14064 (2018).⁹⁰⁸
- [61] M.-S. Zhan *et al.*, ZAIGA: Zhaoshan Long-baseline Atom⁹⁰⁹
 846 Interferometer Gravitation Antenna, Int. J. Mod. Phys.⁹¹⁰
 847 D **29**, 1940005 (2019), arXiv:1903.09288 [physics.atom-⁹¹¹
 848 ph].⁹¹²
- [62] C. Schubert, D. Schlippert, S. Abend, E. Giese, A. Roura,⁹¹³
 849 W. P. Schleich, W. Ertmer, and E. M. Rasel, Scalable,⁹¹⁴
 850 symmetric atom interferometer for infrasound gravita-⁹¹⁵
 851 tional wave detection (2019), arXiv:1909.01951 [quant-⁹¹⁶
 852 ph].⁹¹⁷
- [63] B. Canuel, S. Abend, P. Amaro-Seoane, F. Badaracco,⁹¹⁸
 853 Q. Beaufils, A. Bertoldi, K. Bongs, P. Bouyer, C. Brax-⁹¹⁹
 854 maier, W. Chaibi, N. Christensen, F. Fitzek, G. Flouris,⁹²⁰
 855 N. Gaaloul, S. Gaffet, C. L. G. Alzar, R. Geiger,⁹²¹
 856 S. Guellati-Khelifa, K. Hammerer, J. Harms, J. Hin-⁹²²
 857 derer, M. Holynski, J. Junca, S. Katsanevas, C. Klempf,⁹²³
 858 C. Kozanitis, M. Krutzik, A. Landragin, I. L. Roche,⁹²⁴
 859 B. Leykauf, Y.-H. Lien, S. Loriani, S. Merlet, M. Mer-⁹²⁵
 860 zougui, M. Nofrarias, P. Papadakos, F. P. dos San-⁹²⁶
 861 tos, A. Peters, D. Plexousakis, M. Prevedelli, E. M.⁹²⁷
 862 Rasel, Y. Register, S. Rosat, A. Roura, D. O. Sabulsky,⁹²⁸
 863 V. Schkolnik, D. Schlippert, C. Schubert, L. Sidorenkov,⁹²⁹
 864 J.-N. Siemß, C. F. Sopuerta, F. Sorrentino, C. Struck-⁹³⁰
 865 mann, G. M. Tino, G. Tsagkatakis, A. Viceré, W. von Kl-⁹³¹
 866 itzing, L. Woerner, and X. Zou, Elgar—a european labo-⁹³²
 867 ratory for gravitation and atom-interferometric research,⁹³³
 868 Classical and Quantum Gravity **37**, 225017 (2020).⁹³⁴
- [64] L. Badurina, E. Bentine, D. Blas, K. Bongs, D. Borto-⁹³⁵
 872 letto, T. Bowcock, K. Bridges, W. Bowden, O. Buch-⁹³⁶
 873 mueller, C. Burrage, J. Coleman, G. Elertas, J. Ellis,⁹³⁷
 874 C. Foot, V. Gibson, M. Haehnelt, T. Harte, S. Hedges,⁹³⁸
 875 R. Hobson, M. Holynski, T. Jones, M. Langlois, S. Lel-⁹³⁹
 876 louch, M. Lewicki, R. Maiolino, P. Majewski, S. Malik,⁹⁴⁰
 877 J. March-Russell, C. McCabe, D. Newbold, B. Sauer,⁹⁴¹
 878 U. Schneider, I. Shipsey, Y. Singh, M. Uchida, T. Valen-⁹⁴²
 879 zuela, M. van der Grinten, V. Vaskonen, J. Vossebeld,⁹⁴³
 880 D. Weatherill, and I. Wilmut, Aion: an atom interferom-⁹⁴⁴
 881 eter observatory and network, Journal of Cosmology and
 882 Astroparticle Physics **2020** (05), 011.⁹⁴⁵
- [65] H. Ahlers, L. Badurina, A. Bassi, B. Battelier, Q. Beau-⁹⁴⁷
 883 fils, K. Bongs, P. Bouyer, C. Braxmaier, O. Buch-⁹⁴⁸
 884 mueller, M. Carlesso, E. Charron, M. L. Chiofalo,⁹⁴⁹
 885 R. Corgier, S. Donadi, F. Droz, R. Ecoffet, J. Ellis,⁹⁵⁰
 886 F. Esteve, N. Gaaloul, D. Gerardi, E. Giese, J. Grosse,⁹⁵¹
 887 A. Hees, T. Hensel, W. Herr, P. Jetzer, G. Kleinsteenberg,⁹⁵²
 888 C. Klempf, S. Lecomte, L. Lopes, S. Loriani, G. Métris,⁹⁵³
 889 T. Martin, V. Martín, G. Müller, M. Nofrarias, F. P. D.⁹⁵⁴
 890 Santos, E. M. Rasel, A. Robert, N. Saks, M. Salter,⁹⁵⁵
 891 D. Schlippert, C. Schubert, T. Schuldt, C. F. Sopuerta,⁹⁵⁶
 892 C. Struckmann, G. M. Tino, T. Valenzuela, W. von Klitz-⁹⁵⁷
 893 ing, L. Wörner, P. Wolf, N. Yu, and M. Zelan, Ste-quest:⁹⁵⁸
 894 Space time explorer and quantum equivalence principle⁹⁵⁹
 895 space test (2022), arXiv:2211.15412 [physics.space-ph].⁹⁶⁰
- [66] Y. A. El-Neaj, C. Alpigiani, S. Amairi-Pyka, H. Araújo,⁹⁶¹
 896 A. Balaž, A. Bassi, L. Bathe-Peters, B. Battelier,⁹⁶²
 897 A. Belić, E. Bentine, J. Bernabeu, A. Bertoldi, R. Bing-⁹⁶³
 900 ham, D. Blas, V. Bolpasi, K. Bongs, S. Bose, P. Bouyer,⁹⁶⁴
 901 T. Bowcock, W. Bowden, O. Buchmueller, C. Bur-⁹⁶⁵
 902 rage, X. Calmet, B. Canuel, L.-I. Caramete, A. Car-⁹⁶⁶
 903 roll, G. Celli, V. Charmandaris, S. Chattopadhyay,⁹⁶⁷
 904 X. Chen, M. L. Chiofalo, J. Coleman, J. Cotter, Y. Cui,⁹⁶⁸
 905 A. Derevianko, A. De Roeck, G. S. Djordjevic, P. Dor-⁹⁶⁹
- nan, M. Doser, I. Drougkakis, J. Dunningham, I. Dutan,
 913 S. Easo, G. Elertas, J. Ellis, M. El Sawy, F. Fassi, D. Fe-
 914 lea, C.-H. Feng, R. Flack, C. Foot, I. Fuentes, N. Gaaloul,
 915 A. Gauguet, R. Geiger, V. Gibson, G. Giudice, J. Gold-
 916 win, O. Grachov, P. W. Graham, D. Grasso, M. van
 917 der Grinten, M. Gündogan, M. G. Haehnelt, T. Harte,
 918 A. Hees, R. Hobson, J. Hogan, B. Holst, M. Holyn-
 919 ski, M. Kasevich, B. J. Kavanagh, W. von Klitzing,
 920 T. Kovachy, B. Krikler, M. Krutzik, M. Lewicki, Y.-
 921 H. Lien, M. Liu, G. G. Luciano, A. Magnon, M. A.
 922 Mahmoud, S. Malik, C. McCabe, J. Mitchell, J. Pahl,
 923 D. Pal, S. Pandey, D. Papazoglou, M. Paternostro,
 924 B. Penning, A. Peters, M. Prevedelli, V. Puthiya-
 925 Veettil, J. Quenby, E. Rasel, S. Ravenhall, J. Ringwood,
 926 A. Roura, D. Sabulsky, M. Sameed, B. Sauer, S. A.
 927 Schäffer, S. Schiller, V. Schkolnik, D. Schlippert, C. Schu-
 928 bert, H. R. Sfar, A. Shayeghi, I. Shipsey, C. Signorini,
 929 Y. Singh, M. Soares-Santos, F. Sorrentino, T. Sum-
 930 ner, K. Tassis, S. Tentindo, G. M. Tino, J. N. Tins-
 931 ley, J. Unwin, T. Valenzuela, G. Vasilakis, V. Vasko-
 932 nen, C. Vogt, A. Webber-Date, A. Wenzlawski, P. Wind-
 933 passinger, M. Woltmann, E. Yazgan, M.-S. Zhan, X. Zou,
 934 and J. Zupan, Aedge: Atomic experiment for dark matter
 935 and gravity exploration in space, EPJ Quantum Technol-
 936 ogy **7**, 10.1140/epjqt/s40507-020-0080-0 (2020).
- [67] Y. Du, C. Murgui, K. Pardo, Y. Wang, and K. M. Zurek,
 937 Atom interferometer tests of dark matter, Phys. Rev. D
 938 **106**, 095041 (2022).
- [68] L. Badurina, V. Gibson, C. McCabe, and J. Mitchell,
 939 Ultralight dark matter searches at the sub-hz frontier
 940 with atom multigradiometry, Phys. Rev. D **107**, 055002
 941 (2023).
- [69] S. Chu, J. E. Bjorkholm, A. Ashkin, J. P. Gordon, and
 942 L. W. Hollberg, Proposal for optically cooling atoms to
 943 temperatures of the order of 10^{-6} k, Optics Letters **11**,
 944 73 (1986).
- [70] R. Corgier, S. Amri, W. Herr, H. Ahlers, J. Rudolph,
 945 D. Guéry-Odelin, E. M. Rasel, E. Charron, and
 946 N. Gaaloul, Fast manipulation of bose-einstein condensates
 947 with an atom chip, New J. Phys. **20**, 055002 (2018).
- [71] A. Herbst, T. Estrampes, H. Albers, V. Vollenkemper,
 948 K. Stolzenberg, S. Bode, E. Charron, E. M.
 949 Rasel, N. Gaaloul, and D. Schlippert, Creating nearly
 950 heisenberg-limited matter-waves exploiting tunable inter-
 951 actions (2023), arXiv:2307.06766 [cond-mat.quant-gas].
- [72] S. Kirkpatrick, C. D. Gelatt, and M. P. Vecchi, Optimiza-
 952 tion by simulated annealing, Science **220**, 671 (1983).
- [73] J. Catani, P. Maioli, L. De Sarlo, F. Minardi, and M. In-
 953 guscio, Intense slow beams of bosonic potassium isotopes,
 954 Phys. Rev. A **73**, 033415 (2006).
- [74] A. Herbst, H. Albers, K. Stolzenberg, S. Bode, and
 955 D. Schlippert, Rapid generation of all-optical ^{39}K bose-
 956 einstein condensates using a low-field feshbach resonance,
 957 Phys. Rev. A **106**, 043320 (2022).
- [75] H. Albers, *Time-averaged optical potentials for creat-
 958 ing and shaping Bose-Einstein condensates*, Ph.D. thesis,
 959 Leibniz Universität Hannover (2020).
- [76] G. Salomon, L. Fouché, P. Wang, A. Aspect, P. Bouyer,
 960 and T. Bourdel, Gray-molasses cooling of ^{39}K to a high
 961 phase-space density, EPL (Europhysics Letters) **104**,
 962 63002 (2013).
- [77] C. D'Errico, M. Zaccanti, M. Fattori, G. Roati, M. Ingus-
 963 cito, G. Modugno, and A. Simoni, Feshbach resonances in
 964 ultracold ^{39}K , New Journal of Physics **9**, 223 (2007).

- [78] M. Landini, S. Roy, G. Roati, A. Simoni, M. Inguscio,⁹⁹⁸
G. Modugno, and M. Fattori, Direct evaporative cooling⁹⁹⁹
of ³⁹K atoms to bose-einstein condensation, Phys. Rev.¹⁰⁰⁰
A **86**, 033421 (2012).
- [79] Y. Castin and R. Dum, Bose-einstein condensates in¹⁰⁰¹
time dependent traps, Physical Review Letters **77**, 5315¹⁰⁰²
(1996).
- [80] Y. Kagan, E. L. Surkov, and G. V. Shlyapnikov, Evolution¹⁰⁰⁴
of a bose gas in anisotropic time-dependent traps,¹⁰⁰⁵
Phys. Rev. A **55**, R18 (1997).
- [81] C. J. Pethick and H. Smith, *Bose-Einstein Condensation*¹⁰⁰⁷
in Dilute Gases, 2nd ed. (Cambridge University Press)¹⁰⁰⁸
2008).
- [82] V. M. Pérez-García, H. Michinel, J. I. Cirac, M. Lewenstein,¹⁰⁰⁹
and P. Zoller, Low energy excitations of a bose-einstein¹⁰¹⁰
condensate: A time-dependent variational analysis,
Phys. Rev. Lett. **77**, 5320 (1996).
- [83] V. M. Pérez-García, H. Michinel, J. I. Cirac, M. Lewenstein,¹⁰¹¹
and P. Zoller, Dynamics of bose-einstein condensates:¹⁰¹²
Variational solutions of the gross-pitaevskii equations,
Phys. Rev. A **56**, 1424 (1997).

ACKNOWLEDGEMENTS

We thank Dorothee Tell for thorough proof reading.¹⁰¹⁹ This work is funded by the German Space¹⁰²⁰
Agency (DLR) with funds provided by the Federal Ministry¹⁰²¹
for Economic Affairs and Climate Action due to¹⁰²²
an enactment of the German Bundestag under Grant¹⁰²³
No. DLR 50WM2041 (PRIMUS-IV), 50WM2253A (AI¹⁰²⁴

Quadrat) and supported by the “ADI 2022” project founded by the IDEX Paris-Saclay, ANR-11-IDEX-0003-02. The authors further acknowledge support by the Federal Ministry of Education and Research (BMBF) through the funding program Photonics Research Germany under contract number 13N14875 and by the Deutsche Forschungsgemeinschaft (DFG, German Research Foundation)-Project-ID 274200144—the SFB 1227 DQ-mat within Project No. A05 and B07 and under Germany’s Excellence Strategy—EXC-2123 QuantumFrontiers—Project-ID 390837967.

AUTHOR CONTRIBUTIONS

A.H., H.A., S.B., E.M.R. and D.S. designed the experimental setup and the dipole trapping laser system. A.H., H.A., S.B., K.S., E.M.R. and D.S. contributed to the design, operation, and maintenance of the overall setup. T.E., R.C., E.C. and N.G. set the theoretical framework of this work. A.H., T.E. and H.A. with support of R.C., E.C. and N.G. performed the analysis of the data presented in this manuscript. A.H., T.E. and R.C. with support of D.S., E.C., E.M.R. and N.G. drafted the initial manuscript. All authors discussed and evaluated the results and contributed to, reviewed, and approved of the manuscript.

COMPETING INTERESTS

All authors declare no competing interests.